Environment Technology and Science Journal, 2007, Vol.2 No.1, 60 - 82

Seismic Refraction Investigation of the Subsurface Structure at Ahmadu Bahago Senior Secondary School, Minna, Nigeria

Alfa I.A., *Adeniyi J.O., *Udensi E.E., and *Jonah S.A.

College of Education, Minna, Nigeria

* Department of Physics, Federal University of Technology, Minna, Nigeria

Abstract

A refraction survey was conducted over an area of ½ km x ½ km at the Ahmadu Bahago Senior Secondary School, Minna, in order to study the nature of the geological features and to determine possible aquifer locations. A total of thirty-six points were shot, and analysis of the recorded data was based on the study of velocity pattern from the time-distance graph obtained from the field data. Usually, high-velocity values correspond to high-density materials at increasing depths. Two layers were identified, the first having velocities ranging from 714.29 ms^{-1} to 1666.6 ms^{-1} and the second having velocities ranging from 3267.97 ms^{-1} to 7500 ms^{-1}. The refractor is situated at a depth ranging from 3.33m to 9.63m. The refractor velocities are likely associated with granite-granodiorite and granite-gneiss rocks.

Keywords: Seismic, profile, aquifer, refractor, overburden

Introduction

Detailed surface mapping of the larger area encompassing the present study area had been carried out (Falconer, 1911; Oyawoye, 1964; McCurry 1976; Russ, 1957; Ajibade *et al.*, 1987). But this study is concerned with the description of the subsurface geology by use of a geophysical technique. By this means the depths to basement across the study area can be adequately mapped and points in the subsurface that are favourable for aquifer formation can also be identified. The study covered an area of 1/2km x 1/2km and is situated on the expanse of land belonging to the Ahmadu Bahago Senior Secondary School, Minna, beginning from the Minna-Bosso Road axis and extending out to the Abattoir Road. Network of footpaths in the study area facilitated access from one shot point to the next. The geophysical method that was used in this survey is the seismic method whence seismic or sound waves that are generated on the surface using explosives, hammer blows, or by dropping dead weights are sent into the ground. By this means the earth materials are caused to vibrate due to their elasticity and the resultant motion is detected by geophones. These detecting instruments then send the signals to recording devices. The interest

here is the measurement of arrival times to the geophones from the source of seismic waves. Since much of the earth is elastic solid, two kinds of body waves can be recognized, viz:

* Compression or P-waves, also known as primary arrivals since they arrive first at the recording stations.

* Shear or S-waves, also known as secondary arrivals because their velocities are less than those of P-waves and they arrive at recoding stations later than P-waves (Stacey, 1977; Telford *et al.*, 1976). In addition to the body waves, there are surface waves (often called ground roll) that propagate around the boundaries between layers of different materials or in strong velocity and density gradients near the surface of the earth. A type of surface waves, Rayleigh waves, propagate at the surface of a homogeneous medium; they are non-dispersive, low velocity, low frequency surface wave whose wave motion is such that the paths of the particles of the medium are ellipses whose axes are normally vertical and the minor axes are in the direction of the wave propagation. Rayleigh waves are guided in a surface waveguide in which velocity and density increase downward (Stacey, 1977). The other type of surface waves, Love waves, are always dispersive with velocity increasing with wavelength and are observed only when there is a low velocity layer overlying a higher velocity substratum (Dobrin and Savit, 1988). In seismic survey work, the body waves (i.e. P and S waves) are mostly used because they always arrive at the detectors before the surface waves. Also, surface waves from distant shallow sources normally arrive with much larger amplitudes than the body waves. The energy of such waves is spread along an expanding line around the earth and so constitutes noise; this is unlike the body waves whose wavefront is an expanding surface and thus its amplitude diminishes more rapidly with distance (Stacey, 1977).

In refraction seismic exploration, the most dominant and important wave for interpretation is the P-wave. This is due to the fact that the compressional velocity is always greater than the shear velocity in a given medium and so P-waves are the first easily recognized arrivals. Another reason may be that the earth core, being liquid medium, cannot sustain shear deformation since the shear modulus or rightly of liquid in zero. Simply put, S-wave does not travel through a liquid. Another advantage of using P-waves may be that the motion of the medium in which compressional or P-wave travels is longitudinal, so that there is no polarization of P-waves. However, S-wave, being transverse, is polarized and it becomes necessary to distinguish vertical and horizontal polarisation;

because of such polarisation effect the S-wave behaves differently at sharp horizontal boundaries thereby making the recording and interpretation very difficult. The velocity of S-wave ranges from zero up to 70% of the P-way velocity (Telford et al., 1976; Stacey, 1977; Dobrin and Savit, 1988). In refraction seismic survey, the detector records seismic signals from the shot point. The times required to travel various source-detector distances are recorded and this give information on the velocities (the most important propagation characteristics of seismic waves) and depths of the surface formation along which they propagate. The velocity of seismic waves traveling through a homogeneous solid medium with little or no porosity is a function of the density and the elastic properties of the materials making up the medium. For solids rocks which have more complex microstructures and pore spaces, the actual velocity is very much dependent upon the intrinsic velocity of the minerals constituting the solid rock matrix, the porosity, the pressure, and the velocity of the fluid filling the pore spaces. It also depends on the composition of any solid cementing materials between the grains of the primary rock constituents (Dobrin and Sarvit, 1988).

Seismic velocities in rocks increase generally with depth. But in sedimentary region it depends on pressures from the overburden, which increases the consolidation of the underlying materials. Beyond the consolidation layer, the influence of pressure on velocity becomes small, and then the porosity and mineral composition of the grains becomes dominant. This is the case of rock with more complex microstructures with the space between grains that may contain fluid or softer types of solid material such as clay. Most igneous and metamorphic rocks however have little or no porosity and so, the velocity of seismic waves depend mainly on the elastic properties of the minerals making up the rock material itself. Seismic velocity information can be converted to rock type information that can be used in identifying subsurface materials. It is, however, unwise to rely completely on seismic velocity estimation to the complete exclusion of other factors because the velocities of various rock types vary over wide ranges and even overlaps in rocks. But within a small study area the range of velocity for a particular rock is generally small and so certain rock types can be identified on the basis of velocity (Langston, 1990). Table 1 shows the values of the seismic velocities of some rocks.

Table 1: Measured seismic velocities in some rocks

Rock type	Velocity (ms^{-1})
Alluvium	350 – 2000
Clay	0 – 2500
Dry sand / gravel	500 – 1000
Sandstone	1000 – 4300
Limestone	1700 – 4200
Shale	1000 – 4300
Granite	~ 7700
Gneiss	3500 – 7500
Metamorphic rock	3000 - 7700

Geology of the Study Area

The region of the area of study was first visited by Falconer during his reconnaissance survey of Northern Nigeria (Falconer, 1911). He identified the main rock types to be older granite, schist, and the migmatite gneiss complex. He further described the quartzite, quartzite-schist, hornblende schist and feldspathic gneiss in Minna and its environs and observed that the different rocks are often arranged in alternating parallel bands. Russ mapped the area as part of a much larger area in the old Zaria, Niger, and Sokoto provinces (Russ, 1957). Ajibade did a detailed mapping of the Minna sheet that include the present area and classified the rock types into schist, granite, and gneiss (Ajibade, 1987). Udensi et al (1986) did an analysis of the density of the rocks in the Minna Area and found that the rock types in the region include migmatite-gneiss, schists, granites and quartzites. But most of the granites in the area of study are older granites and are distinguished from the younger granites found in the Jos Area. Generally, the rocks of this area are of metamorphic and igneous origin and some of them formed continuous ridges of steep-sided hills. The study area is also characterized by lowlands and drained by marshes while the soil texture is

mostly coarse-grained and whitish in colour. Fig.1 is a geological sketch map of the larger area containing the principal area of study.

The Geophysical Survey

Instrumentation: The seismic refraction survey was performed with the aid of a 3-channel enhancement seismograph (Mod. 579). The full package comprises of three units of geophone, hammer and aluminum plate, and a length of cable. The geophone is the unit that detects signals and is in direct contact with the earth. The seismic energy is generated using an 8.9kg hammer that strikes an aluminium plate placed directly at the designated shot point. The hammer is connected to the recording device by a cable; this is necessary in order for the recording unit to detect the instant at which the hammer strikes the plate. This initial time record is then the reference or zero-second time from which times of travel of the seismic waves thus generated are compared. The seismograph is a computerized recording system that processes data before they are presented on a visual display unit. The geophones are connected directly to the seismograph by cables that transmit signals that are processed and displayed as arrivals on the seismograph.

Data Acquisition: A total of six profiles were cut for the survey, and the profile layout is shown in Fig. 2. The survey crew was divided into three groups for ease of work; the first group laid cables and fixed geophones to the ground, the second group was in charge of hammering, and the third group recorded the data. More than one set of data was recorded at each shot point except where one kink was noticed. The different units of the recorder system were always tested and adjusted for good operation and recording. Profiling enables a surveyor to define the appropriate shot point. A total of six profiles were traced. In Fig.2, the first profile was labeled ‘A'. A total of six shot points were located, pegged and labeled as A_0, A_1 A_2, A_3, A_4, and A_5 with 100m spacing between two consecutive shot points along the profile. The second profile, labeled 'B', was exactly 100m from profile A on which six shot points were also located and labeled B_0 to B_5. This was followed by profiles C, D, E and F. And on each profile six shot point were located as shown in Fig.2. The geophone separation was fixed at 10m.

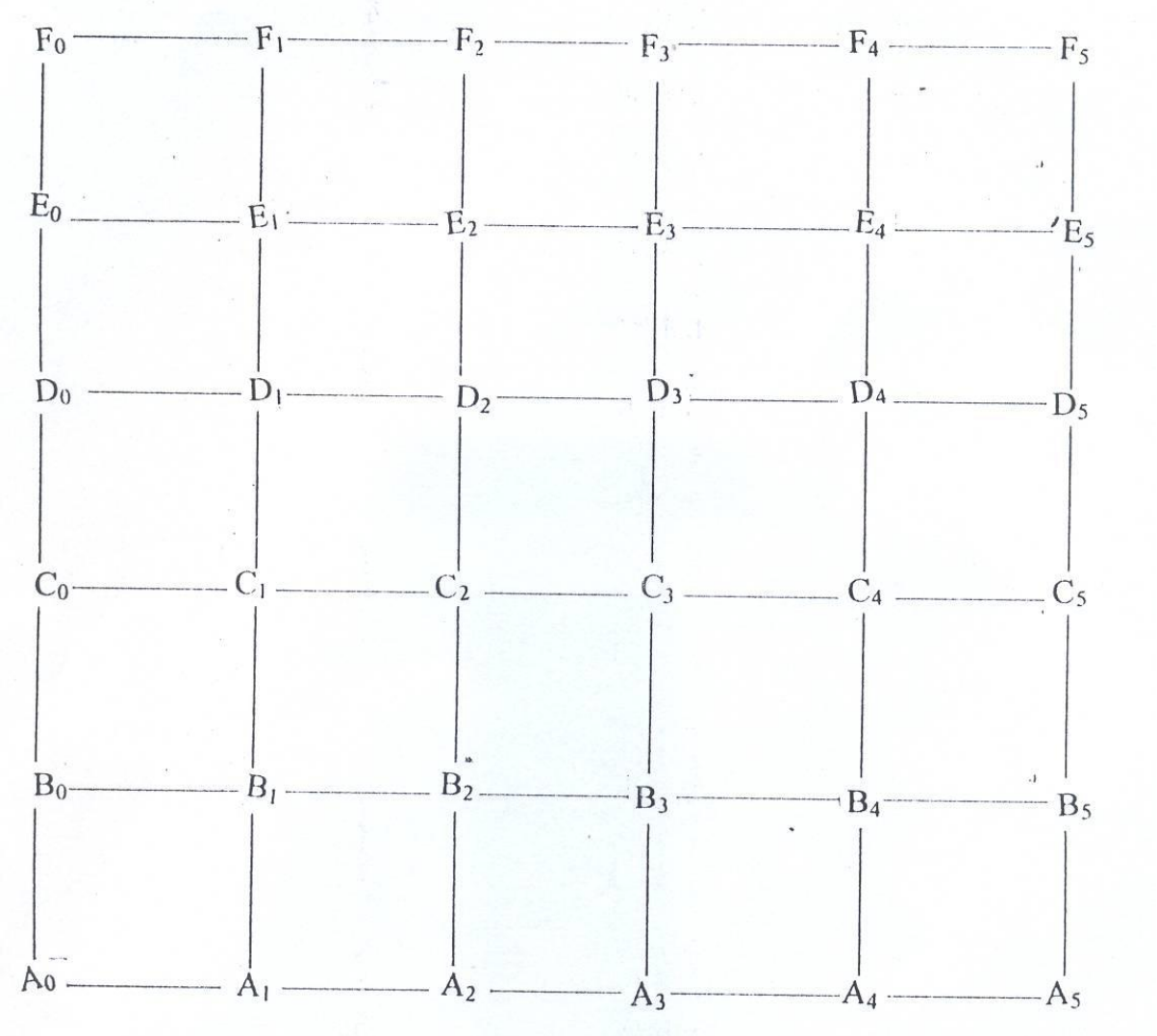

Fig .2: Profile layout

Results: The data corresponding to the arrival times in milliseconds are presented in Tables 1-6.

Table 1: Field Data for Profile A

Hammering Points	**Arrival times (msec)**					
	G1 (10m)	G2 (20m)	G3 (30m)	G4(40m)	G5 (50m)	G6 (60m)
A_0	15.0	18.0	20.0	21.4	22.0	25.0
A_1	5.0	15.0	17.0	19.0	20.0	22.0
A_2	8.0	12.0	16.0	16.5	19.2	24.0
A_3	10.0	17.0	18.0	19.0	22.0	24.0
A_4	11.0	16.8	Null reading	20.4	22.0	24.0
A_5	12.0	15.0	18.0	20.0	21.0	24.0

Table 2: Field Data for Profile B

Hammering Points	**Arrival times (msec)**					
	G1 (10m)	G2 (20m)	G3 (30m)	G4 (40m)	G5 (50m)	G6 (60m)
B_0	6.5	12.0	17.0	18.7	20.5	24.4
B_1	6.0	13.0	15.6	20.0	22.0	25.0
B_2	8.0	15.0	19.0	21.7	Null reading	24.7
B_3	9.0	16.0	19.5	20.7	22.0	24.0
B_4	10.0	18.0	19.0	21.0	23.0	24.5
B_5	8.0	15.0	17.0	19.0	22.0	25.0

Table 3: Field Data for Profile C

Hammering Points	**Arrival times (msec)**					
	G1 (10m)	G2 (20m)	G3 (30m)	G4 (40m)	G5 (50m)	G6 (60m)
C_0	9.0	18.0	19.0	22.0	23.9	24.5
C_1	11.2	13.0	16.8	19.9	21.0	23.9
C_2	8.0	17.0	19.3	21.0	22.8	24.5
C_3	9.0	10.0	12.5	15.5	19.0	22.5
C_4	8.8	18.0	19.0	20.1	22.0	24.6
C_5	14.0	15.6	18.0	22.0	23.5	25.0

Table 4: Field Data for Profile D

Hammering Points	**Arrival times (msec)**					
	G1 (10m)	G2 (20m)	G3 (30m)	G4 (40m) .0	G5 (50m)	G6 (60m)
D_0	10.0	17.0	19.0	20.5	22.0	23.3
D_1	12.0	15.0	17.0	18.5	19.0	20.6
D_2	9.0	17.0	20.0	22.0	23.6	24.5
D_3	9.0	15.0	19.0	21.7	23.1	24.5
D_4	7.1	12.8	15.0	19.1	22.0	24.3
D_5	9.0	16.1	18.0	20.5	22.8	24.3

Table 5: Field Data for Profile E

Hammering Points	**Arrival times (msec)**					
	G1 (10m)	G2 (20m)	G3 (30m)	G4 (40m)	G5 (50m)	G6 (60m)
E_0	7.4	12.0	15.6	18.0	21.0	22.5
E_1	10.0	16.0	18.5	21.0	23.0	24.5
E_2	5.5	12.0	16.0	18.0	20.0	22.0
E_3	10.2	18.0	20.5	21.0	22.6	24.8
E_4	11.4	18.8	20.6	23.0	24.0	24.6
E_5	7.0	12.1	17.0	20.5	22.0	22.6

Table 6: Field Data for Profile F

Hammering Points	**Arrival times (msec)**					
	G1 (10m)	G2 (20m)	G3 (30m)	G4 (40m)	G5 (50m)	G6 (60m)
F_0	6.9	11.9	14.0	16.9	18.0	19.6
F_1	11.0	17.4	19.0	21.3	23.3	24.5
F_2	11.7	15.2	18.1	20.5	23.5	25.0
F_3	8.1	12.4	15.2	17.7	21.0	23.4
F_4	10.0	18.0	20.0	22.0	24.0	25.0
F_5	11.2	14.3	17.0	20.0	23.0	22.6

Data Analysis: The data analysis procedure consists of plotting of graphs based on the recorded data; in this case the arrival time is plotted on the ordinate axis and the geophone distance is plotted on the abscissa axis. The inverse of the slope of two lines are the velocities i.e. the velocity of the first medium v_1 and the velocity of the second medium v_2. These velocity values, in addition to the intercept time, are commonly applied to compute the depth to the refractor of each shot point. The basic assumption here is that we are dealing with flat-lying refractors. According to Kearey and Brooks (1984), in many geological situations subsurface refractors may approximate planar surfaces over the linear extent of a refractor line. In such cases the observed travel-time curves are commonly assumed to derive from a set of planar layers and are analysed to determine the depths to individual planar refractors. The geometry of refracted ray paths through layer models of the subsurface is considered as follows: in Fig.2 the progressive positions of the wavefront associated with energy traveling directly through an upper layer and energy critically refracted in a lower layer from a seismic source at point, say A, is shown. Also shown are direct and refracted ray paths to a detector at another point, say D, a distance x from the source.

Fig.2: Successive positions of the expanding wavefronts for direct and refracted waves through a two-layer model. Individual ray paths from A to detector D are shown.

The layer velocities are v_1 and v_2 ($>v_1$) and the refracting interface is at a depth z. The direct ray travels horizontally through the top of the upper layer from A to D at velocity v_1. The refracted ray travels down to the interface and back up to the surface at velocity v_1 along slant paths AB and CD and is inclined at the critical angle θ, and travels along the interface between B and C at the higher velocity v_2. The total travel time along the refracted ray path ABCD is

$$t = t_{AB} + t_{BC} + t_{CD}$$

$$= z/v_1\cos\theta + (x-2z\tan\theta)/v_2 + z/v_1\cos\theta$$

Noting that $\sin\theta = v_1 / v_2$ (Snell's Law) and $\cos\theta\ (1- v_1^2/v_2^2)^{1/2}$, the travel time equation may be expressed in a number of different forms, a useful general form being

$$t = x\sin\theta/v_1 + 2z\cos\theta/v_1 \qquad (1)$$

Alternatively, $$t = x/v_2 + 2z\,(v_2^2-v_1^2)^{1/2}/\,v_1v_2 \qquad (2)$$

Or $$t = x/v_2 + t_i \qquad (3)$$

where, plotting t against x (Fig.3) , t_i is the intercept on the time axis of a travel-time curve or *time-distance curve* having a gradient of $1/v_2$. The *intercept time,* t_i, is given by

$$t_i = 2z\,(v_2^2-v_1^2)^{1/2}/\,v_1v_2 \qquad (4)$$

Solving for refractor depth from Eq.4

$$z = t_i\, v_1v_2/2(v_2^2-v_1^2)^{1/2} \qquad (5)$$

Thus by analysis of the travel-time curves of direct and refracted arrivals, v_1 and v_2 can be derived (reciprocal of the gradient of the relevant travel-time curve, see Fig.3) and from the intercept time ti the refractor depth z can be determined (Kearey and Brooks, 1984). The computed values of first layer velocity v_1, the refracted velocity v_2, and the depth to refractor z are shown in Tables 7 - 12.

Table 7: Calculated values of v_1 (m/s), v_2 (m/s) and z (m) for Profile A

Hammering Point	First Layer Velocity v_1 (m/s)	Refractor Layer Velocity v_2 (m/s)	Depth to Refractor z (m)
A_0	1111.11	5714.29	8.50
A_l	1333.33	5714.29	7.20
A_2	1250.00	3750.00	4.64
A_3	1000.00	5000.00	5.61
A_4	909.09	5555.56	5.53
A_5	833.33	4166.67	4.25

Table 8: Calculated values of v_1 (m/s), v_2 (m/s) and z (m) for Profile B

Hammering Point	First Layer Velocity v_1 (m/s)	Refractor Layer Velocity v_2 (m/s)	Depth to Refractor z (m)
B_0	1538.46	3508.77	8.13
B_1	1538.46	4000.00	5.83
B_2	1250.00	6666.67	6.68
B_3	1111.11	5000.00	6.27
B_4	1000.00	5714.29	7.11
B_5	1250.00	4000.00	6.58

Table 9: Calculated values of v_1 (m/s), v_2 (m/s) and z (m) for Profile C

Hammering Point	First Layer Velocity v_1 (m/s)	Refractor Layer Velocity v_2 (m/s)	Depth to Refractor z (m)
C_0	1111.11	5454.55	7.94
C_1	892.86	3937.01	4.58
C_2	1250.00	5333.33	8.36
C_3	1111.11	3703.70	4.08
C_4	1136.36	5357.14	6.98
C_5	714.29	4545.45	3.62

Table 10: Calculated values of v_1 (m/s), v_2 (m/s) and z (m) for Profile D

Hammering Point	First Layer Velocity v_1 (m/s)	Refractor Layer Velocity v_2 (m/s)	Depth to Refractor z (m)
D_0	1000.00	6349.21	6.58
D_1	833.33	5813.95	4.21
D_2	1111.11	6666.67	7.89
D_3	1111.11	4210.53	6.34
D_4	1408.45	3478.26	5.01
D_5	1111.11	4878.05	6.28

Table 11: Calculated values of v_1 (m/s), v_2 (m/s) and v (m) for Profile E

Hammering Point	First Layer Velocity v_1 (m/s)	Refractor Layer Velocity v_2 (m/s)	Depth to Refractor z (m)
E_0	1351.35	3809.52	5.78
E_l	1000.00	4705.88	5.12
E_2	1666.67	5000.00	8.84
E_3	1111.11	5263.16	9.09
E_4	877.19	7500.00	7.07
E_5	1428.57	5357.14	9.63

Table 12: Calculated values of v_1 (m/s), v_2 (m/s) and z (m) for Profile F

Hammering Point	First Layer Velocity V_1 (m/s)	Refractor Layer Velocity V_2 (m/s)	Depth to Refractor z (m)
F_0	1449.28	5357.14	5.80
F_l	909.09	5633.80	6.45
F_2	854.70	3759.40	4.39
F_3	1234.56	3267.97	3.33
F_4	1000.00	5714.29	7.62
F_5	892.86	3623.19	9.21

In plotting of graph, it was considered that, at the shot point, the arrival time was assumed to be zero even though no geophone was fixed there. Coherent events were then used to get velocity pattern, which define the direct waves and refracted waves. The trend starting from origins represent the direct waves. The plotted graphs for a section of Profile A are shown in Fig. 3.

Interpretation of Data

Interpretation Procedures and Techniques: The interpretation of seismic refraction data entails the use of the seismic velocity information obtained by processing arrival data in identifying sub-surface materials. Within certain limits, seismic velocity information can be converted to rock type. Information available on velocity of various rocks types (see Table 1) shows that velocities of rock overlap. Therefore, velocity alone cannot be used to specify rock type. To interpret accurately, the interpreter must have a sound knowledge of the geology of the area of study. However, within a small study area, the range of velocity for a particular rock type is generally small, and certain rock types can be identified on the basis of velocity only. Seismic refraction interpretation is often based on the earliest arriving energy on a seismic trace, commonly called the first arrival. This is primarily because of the relative ease of recording, identifying and timing them on the record. Though useful information such as velocities can also be obtained from second arrivals, they are rarely used because of the problems associated with timing them. At offset distances close to the shot point first arrivals indicate direct wave while at larger offsets they indicate refraction from refractors. In the most elementary form of seismic refraction surveying, travel time equations are developed based on simple models of the earth e.g. two-layer and multi-layer cases. These equations are used to develop methods of interpreting data and for generating synthetic anomalies which serve as aid in interpretation and more importantly too, as aid in survey design. The interpretation technique that has been used for many years is the intercept time method. This method assumes a simple model where refractors are planar and have no lateral velocity changes. Thus, when a simple model is assumed, appropriate field procedures capable of yielding the data for the techniques are adopted. If the refractors meet the required criteria, the intercept time method is justified. In general, irregular refracting surface accompanied by lateral velocity changes are probably much more common than planar boundaries with no velocity changes along them. Hence the intercept time method leaves uncertainties in the interpretations where they are employed (Langston, 1990).

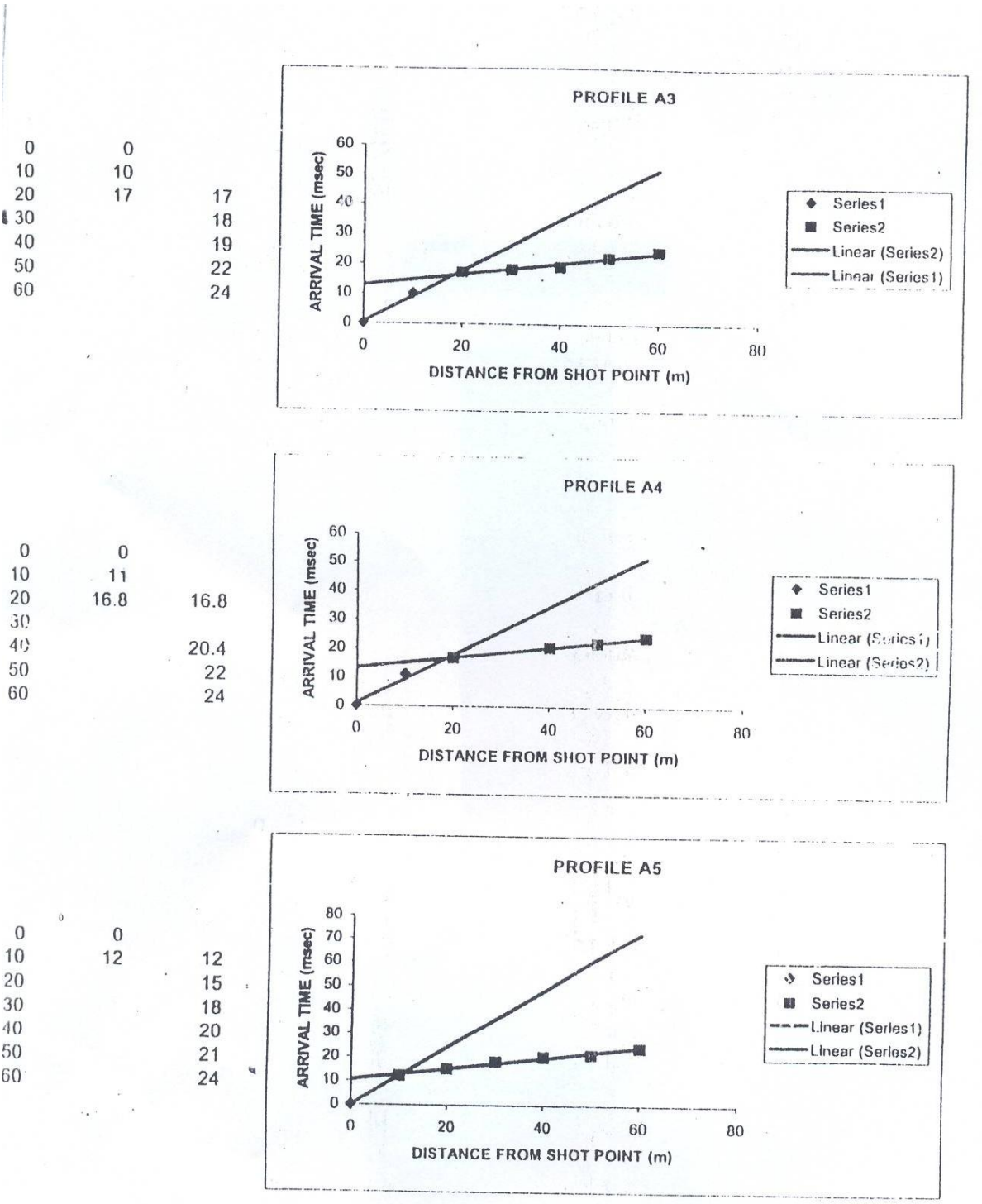

Fig. 3: Plots (i.e. time-distance graph) for a section of Profile A

The overburden layer velocities in metres per second (m/s) are as shown in Table 13. The velocity values for the overburden were contoured and the result is presented in Fig. 4.

Table 13: First layer velocities (m/s)

	SHOT POINTS LOCATION ALONG PROFILE					
PROFILES	0 (m)	100 (m)	200 (m)	300 (m)	400 (m)	500 (m)
A	1111.11	1333.33	1250.00	1000.00	909.09	833.33
B	1538.46	1538.46	1250.00	1111.10	1000.00	1250.00
C	1111.11	892.86	1250.00	1111.10	1136.36	714.29
D	1000.00	833.33	1111.11	1111.10	1408.45	1111.11
E	1351.35	1000.00	1666.67	1111.10	877.19	1428.57
F	1449.28	909.09	854.70	1234.60	1000.00	892.86

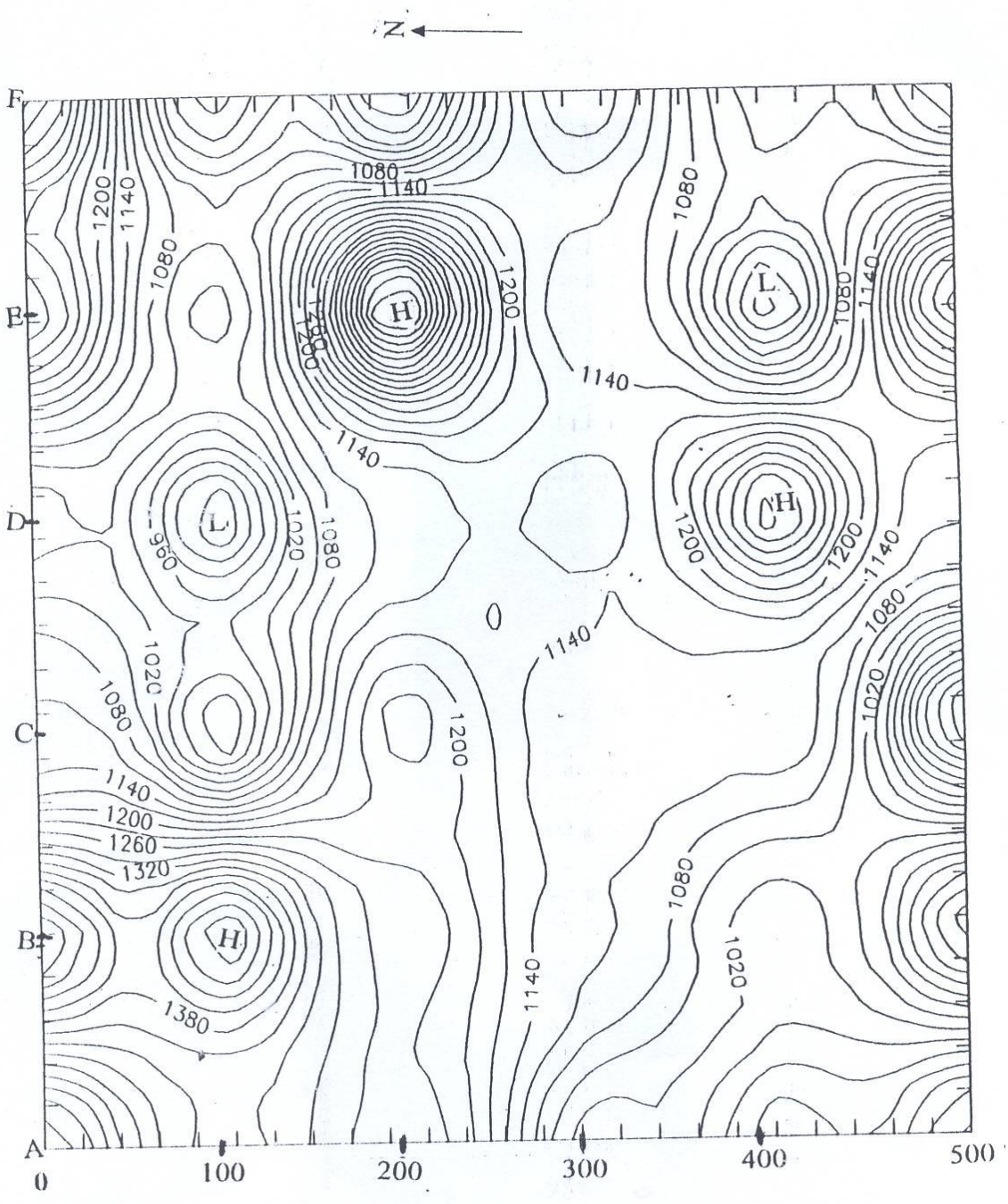

Fig. 4: Contour map of overburden (first layer) velocities (contour interval is 30m/s)

The refractor velocities are as shown in Table 14.

Table 14: Second layer velocities (m/s)

	SHOT POINTS LOCATION ALONG PROFILE					
PROFILE	0 (m)	100 (m)	200 (m)	300 (m)	400 (m)	500 (m)
A	5714.29	5714.29	3750.00	5000.00	5555.56	4166.67
B	3508.77	4000.00	6666.67	5000.00	5714.29	4000.00
C	5454.55	3937.01	5333.33	3703.70	5357.14	4545.45
D	6349.21	5813.95	6666.67	4210.53	3478.26	4878.05
E	3809.52	4705.88	5000.00	5263.16	7500.00	5357.14
F	5357.14	5633.80	3759.40	3267.97	5714.29	3623.19

The velocity values in Table of 14 were contoured and the result presented as Fig.5.

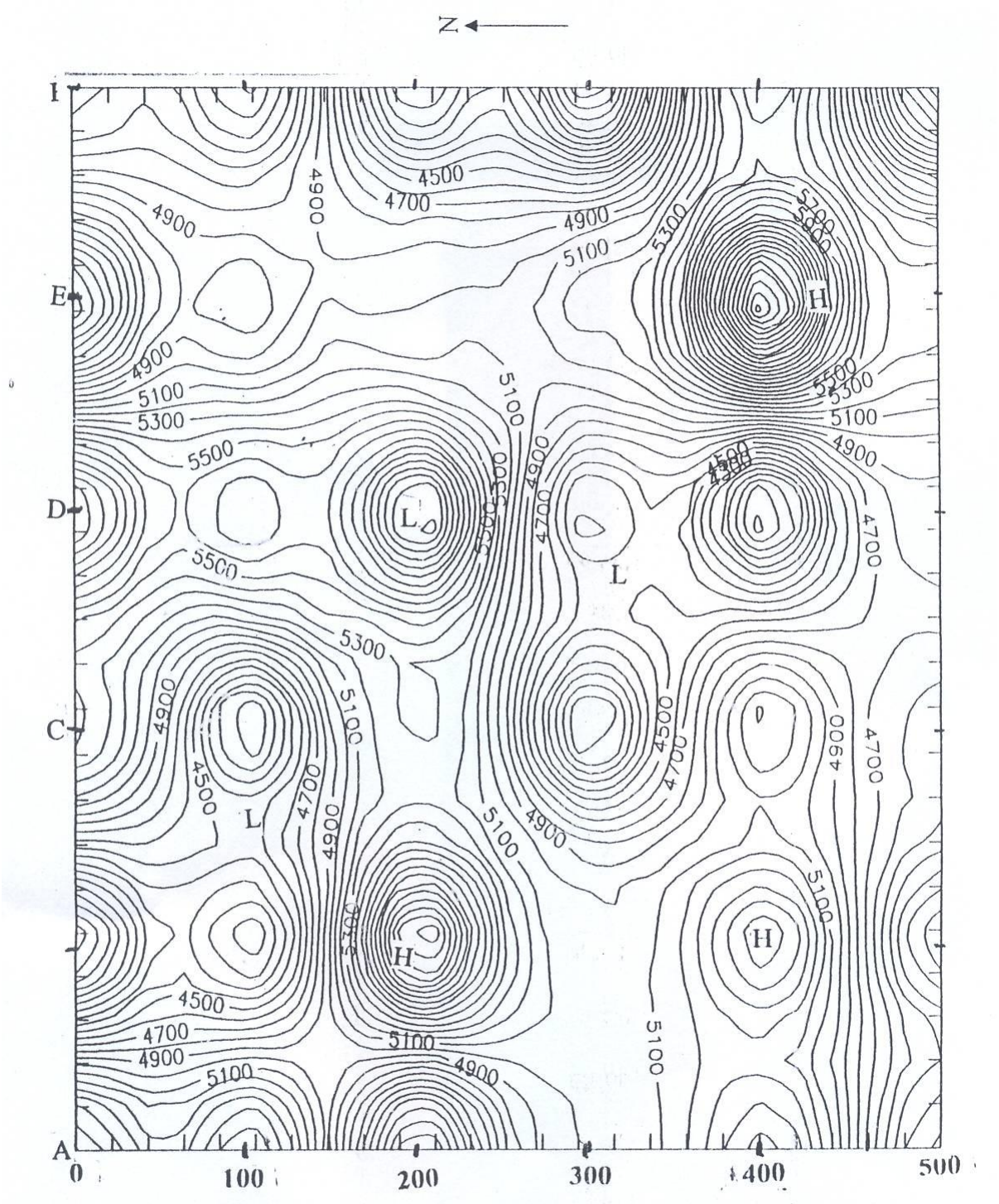

Fig. 5: Contour map of refractor velocities (contour interval is 1000m/s)

Table 15 shows the depth to refractor.

Table 15: Depth to refractor

	SHOT POINTS LOCATION ALONG PROFILE					
PROFILE	0 (m)	100 (m)	200 (m)	300 (m)	400 (m)	500 (m)
A	8.50m	7.20m	4.64m	5.61m	5.53m	4.25m
B	8.13m	5.83m	6.68m	6.27m	7.11m	6.58m
C	7.94m	4.58m	8.36m	4.08m	6.98m	3.62m
D	6.58m	4.21m	7.89m	6.34m	5.01m	6.28m
E	5.78m	5.12m	8.84m	9.09m	7.07m	9.63m
F	5.80m	6.05m	4.39m	3.33m	7.62m	9.21m

The values presented in Table 15 were contoured and the result is presented as Fig. 6.

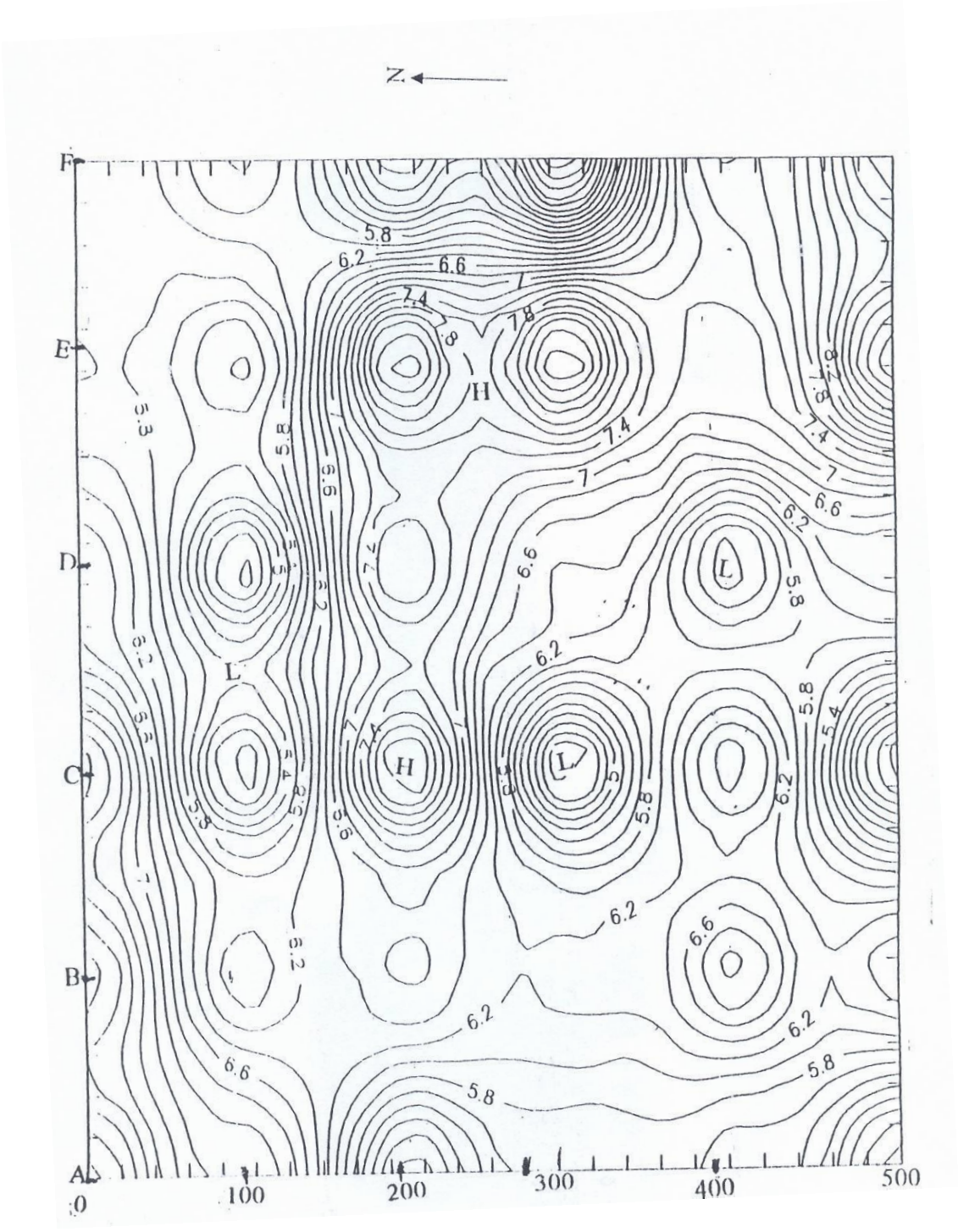

Fig. 5: Contour map of depth to refractor (contour interval = 0.2m)

Discussion

In this study travel times based on first arrivals were recorded. The travel times (in milliseconds) were plotted against geophone spacing to obtain the time-distance graphs; the time-distance graphs reveal two straight-line segments. This revelation simply shows that the survey delineated two seismic layers, viz: an overburden layer and a refractor layer in all six main profiles. It is seen in Table 13 that the least value of the overburden velocity of 714.29m/s is noticed along profile C, and the highest value of overburden velocity of 1666.67m/s is noticed along profile E. In the contour map of Fig.4, the closures designated as H (i.e. highs) are those points where the contour values are increasing inward whereas the closures designated as L (i.e. lows) are those points where the contour values are decreasing inward. In Fig.4, the points with comparatively high overburden velocities occur at approximately B_1, D_4, and E_2 whilst the points with comparatively low overburden velocities occur at D_1 and E_4. Actually, the highest value of overburden velocity of 1666.67m/s is at E_2 but in the contour map of Fig.4 the "L" indicator for the lowest value of 714.29m/s is just outside the margin of the map.

It is seen in Table 14 that the velocity of the refractors ranges from 3267.97m/s to 7500.00m/s on profiles F and E. In the contour map of Fig.5, point H represents areas where the contour values are increasing inward and point L represents areas where the contour value are decreasing inward. Also, the points with comparatively high refractor velocities occur at B_2, B_4, and E_4 whilst comparatively low refractor velocities occur between B_1 and C_1, at D_2, and approximately midway between C_3, D_3, and D_4. The highest value of refractor velocity of 7500m/s is seen at E_4.

It is seen in Table15 that the refractor is deepest at E_5 and shallowest at F_3; the values of Table15 were contoured and the result is shown in Fig.6. In Fig.6, the contour closures marked H are those areas where contour values are increasing inward whilst those marked L are those areas where contour values are decreasing inward. The points marked H are seen to be at C_2, and between E_2 and E_3 in Fig.6. It is instructive to point out that point H also occurs at A_1, E_5, and F_5 but these are not shown in Fig.6 owing to margin constraints. The points of L are seen to be at C_3, between C_1 and D_1, and at D_4; it is also conceivable that point L occur at A_5, F_2, F_3, but these are not shown.

One may wonder what is the significance of the H and L values on a contour map. We posit that on a map where the contour closure trend is not uniform (i.e. all closures decrease inward or all closures increase outward) the highs and lows are merely identification guides.

The variation in the first layer velocity from 714.29m/ to 1666.67m/s is obviously due to an aggregation of different rock types in the area of study. It is a known fact that the type of rocks found in a particular area accounts for the different ranges of seismic velocities of the area. Even when the types of rocks in an overburden are the same, differences in the level of consolidation will translate to differences in seismic velocities. As rocks become deeply buried, their densities increase since their pore space become filled and the constituent minerals are recrystallised in the process of compaction and metamorphism. Thus their seismic velocities increase also (Telford et al., 1976). It can be inferred from Table 1 that different rock types are characterised by range of velocities that actually overlap.

Four profile lines, i.e. A-A^1, B-B^1, C-C^1, and D-D^1, were chosen across the strike of the contour map of Fig.6 for trend analysis as seen in Fig.7. The vertical sections are presented in Fig.8. Along profile A-A^1 (Fig.8a), the deepest point of 8.13m lies at the extreme north end of the profile while the shallowest point of 5.83m is 100m due south of the deepest point. In between these two extremes are the 7.11m depth point due south of the deepest point, the 6.68m, 6.58m, 6.27m and 5.83m depth points located at distances of 200m, 500m, 300m, and 100m respectively from the deepest point. At the 6.68m depth point the seismic velocity is 6666.67m/s, which is a sudden surge above the norm along the refractor of the profile of A-A^1. The overburden velocity at the deepest point is 1538.46m/s; this value corresponds to the lower end of the value of seismic velocity in water-saturated sand, viz: 1500m/s – 2000m/s (Kearey and Brooks, 1984). At all other points the overburden velocities range from 1000m/s – 1250m/s. Along profile B-B^1 (Fig.8b), the deepest point of 8.36m lies 200m due south from the extreme northernmost point while the shallowest point of 3.62m is found at the southernmost end of the profile. In between these two extremes are the 7.94m depth point at the extreme north end of the profile, the 6.98m, 4.58m, and 4.08m depth points located at distances of 200m south of the deepest point, 100m due north of the deepest point, and 100m due south of the deepest point. There is no noticeable surge in the refractor

velocity along this profile. The overburden velocity at the deepest point is 1250m/s, and this velocity value is outside the range of that of water-saturated sand; however, at all other points, the overburden velocities range from 714.29m/s – 1136.36m/s.

Along profile C-C^1 (Fig.8c), the deepest point of 7.89m lies 200m due south from the extreme northernmost point while the shallowest point of 4.21m is located 100m north of the deepest point. In between these two extremes are the 6.58m depth point at the extreme north end of the profile, the 6.34, 6.28m, and 5.01m depth points located at distances of 100m south of the deepest point, 300m due north of the deepest point, and 200m due south of the deepest point. There are noticeable high velocity values in the refractor velocity at the first two deepest points along this profile. The overburden velocity at the deepest point is 1111.11m/s and this velocity value is outside the range of that of water-saturated sand; however, at all other points, the overburden velocities range from 833.33m/s – 1408.45m/s. Along profile D-D^1 (Fig.8d), the deepest point of 9.63m lies at the extreme south end of the profile while the shallowest point of 5.12m is 400m due north of the deepest point. In between these two extremes are the 9.09m depth point 200m due north of the deepest point, the 8.84m, 7.07m, and 5.78m depth points located at distances of 300m due north, 100m due north, and 500m due north (i.e. the northernmost point) from the deepest point. At the 7.07m depth point the seismic velocity is 7500m/s, which is a sudden surge above the norm along the refractor of the profile of D-D^1. The overburden velocity at the deepest point is 1428.57m/s; this value is just shy of the lower limit of the value of seismic velocity in water-saturated sand. At all other points the overburden velocities range from 877.19m/s – 1666.67m/s.

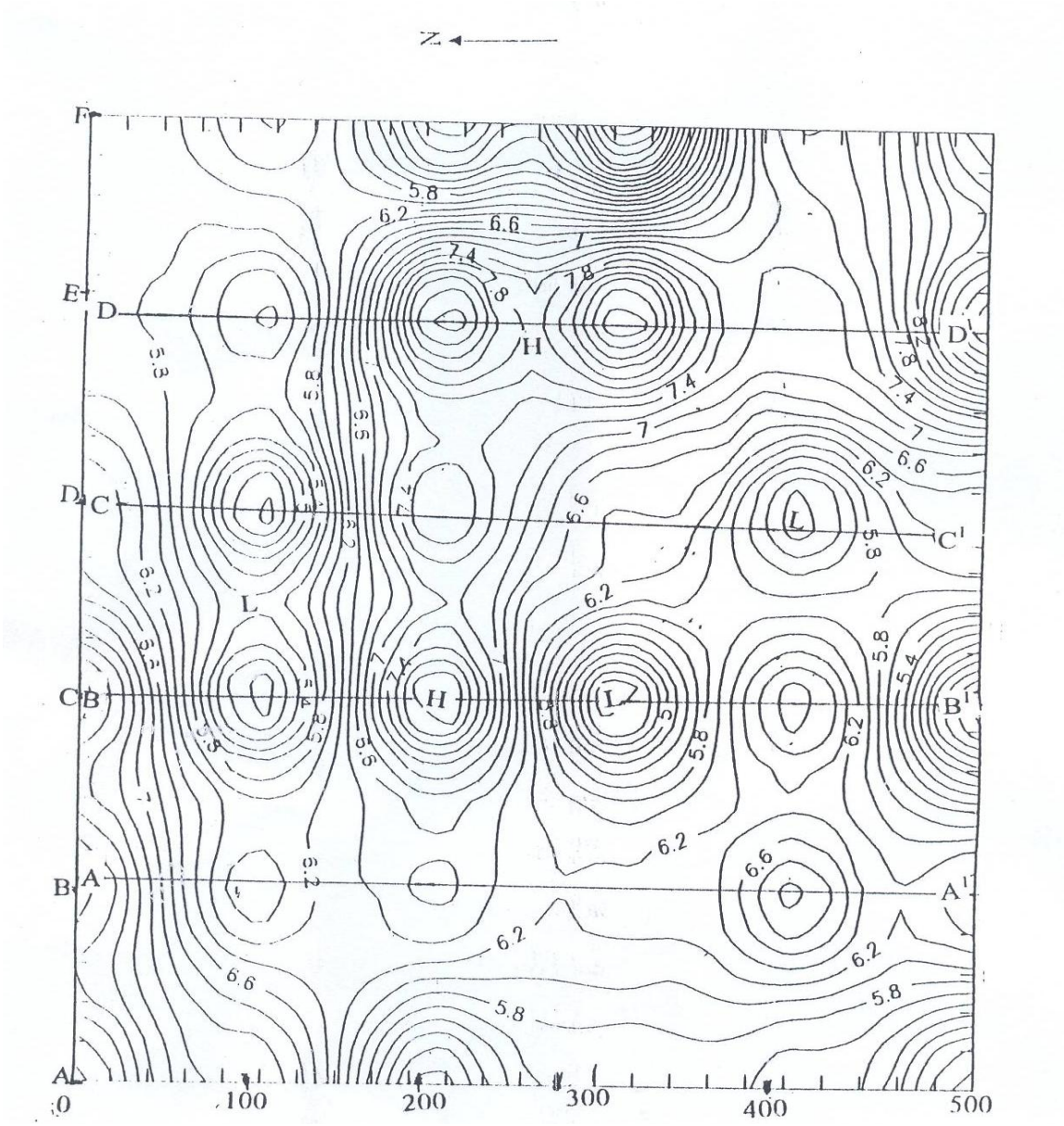

Fig. 7: Contour map of depth of refractor layer showing four profiles taken across the strike of profile (contour interval is 0.2m)

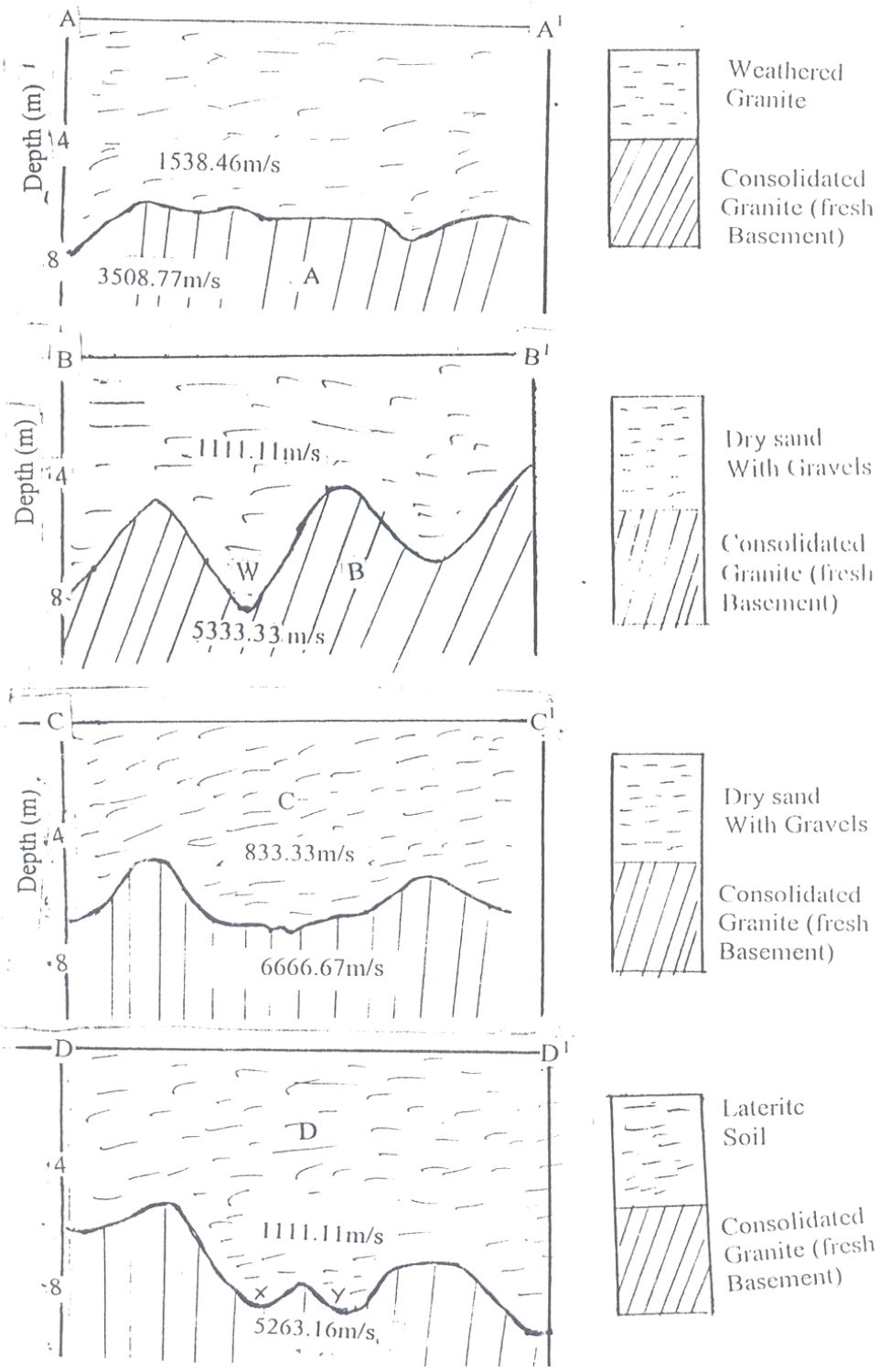

Fig. 8: Vertical Sections of Depth to Refractor

Conclusion

The first layer (overburden) and second layer (or refractor) velocities determined for all segments of the entire area survey indicate to a large extent the rock nature of the area. However, refractor layer velocities obtained vary over the entire area studied. Variation in refractor velocities can be attributed to variations in rock type, composition of mineral assemblages found in the various segments, uneven weathering and complicated histories of metamorphism of the refractor layer. Likewise, variation in the seismic velocity obtained for segments of the first (or overburden) layer can be attributed to variation in the consolidation of the rock materials found within the layer. In conclusion, the granitic rocks which dominate the study area, have little or no porosity, and can only hold only a fraction of water, and the velocity of the refractor layer is also associated with the velocity of consolidated granite rock. Then locating where borehole can be dug here requires looking for points where there is fracture, or thick over burden layer. Since fracture zones of some rock such as granite, basalt and gabbros or places with high overburden layer thickness act as aquifers (Don et at., 1978), it can be concluded that boreholes can be sunk at points marked "W" (Fig. 7b), "X" and "Y" (Fig. 7d) at the central and eastcentral parts respectively of the area. Hand-dug wells observed in the area does not contain plenty water, but does not dry up even during dry season.

Recommendation

It is recommended that looking for site where boreholes can be dug at this surveyed area requires looking for a fracture zone or places where the depth to refractor is high. It is therefore recommended that the points marked "W", "X" and "Y" at the central and east central parts of the survey area are ideal points for sinking boreholes because they are the probable places where water can be found in some reasonable quantity. They may likely constitute a crack in the fresh basement, and this made them to have thick overburden layer. With respect to civil engineering applications, every other point (other than those identified as suitable sites for sinking boreholes) are recommended as appropriate since they are characterized by shallow overburden layers. In addition to the seismic refraction method used in this survey, the resistivity survey could be carried out in area to corroborate the results of this study.

REFERENCES

Ajibade, A.C., Woakes, M., and Rahaman, M.A. 1987. Proterozoic crystal development in the Pan-Africa Regime of Nigeria, *American Geophysical Union*, **25**, 271.

Dobrin, M.B. and Savit, C.H. 1988. *Introduction to Geophysical Prospecting*, McGraw-Hill, New York.

Don, L.L., Sheldon, E., Marvin, K. 1978. *Physical Geology (5ed.)*, Prentice-Hall, New Jersey.

Falconer, J.D. 1911. *The Geology of Northern Nigeria*, Macmillan, London.

Kearey, P. and Brooks, M. 1984. *An Introduction to Geophysical Exploration*, Blackwell Scientific Pblication, Oxford.

Langston, R.W. 1990. High resolution refraction seismic data acquisition and interpretation. In *Geotechnical and Environmental Geophysics*, Ward, S.H., ed., 45-73.

McCurry, P. 1976. The geology of the Precambrian to lower Paleozoic rocks of northern Nigeria. *In Geology of Nigeria*, Kogbe, C.A., ed., Elizabethan, Lagos, 15-39

Oyawoye, M.D. 1964. The geology of the Nigeria basement complex. *Journ. Nig. Min. Geol. Met. Soc.*, **1**, 87-102.

Russ, W. 1957. The geology of part of Nigeria, Zaria, and Sokoto provinces. *Geol. Surv. Nig. Bull*., **27**, 1-42.

Stacey, F. D. 1977. *Physics of the Earth*, John Wiley and Sons, New York.

Telford, N.W., Geldart, L.P., Sheriff, R.S., and Keys, D.A. 1976. *Applied Geophysics*, Cambridge University Press, Cambridge.

Udensi, E.E., Ojo, S.B., and Ajakaiye, D.E. 1986. A three-dimensional interpretation of the Bouguer anomalies over the Minna Batholith in Central Nigeria. *Nig. Precambrian Research*, **32**, 1-15